Photoinduced Electron-Transfer from Mono-/Oligo-1,4-phenylenevinylenes Containing Aromatic Amines to C_{60}/C_{70} and Electron-Mediating Process to Viologen Dication in Polar Solution

Hitoshi Onodera,[†] Yasuyuki Araki,[†] Mamoru Fujitsuka,[†] Shinji Onodera,[†] Osamu Ito,*[,†] Fenglian Bai,[‡] Min Zheng,[‡] and Jun-Lin Yang[‡]

Institute of Multidisciplinary Research for Advanced Materials, Tohoku University, CREST, Japan Science and Technology Corporation, Katahira, Aoba-ku, Sendai 980-8577, Japan; and Laboratory of Organic Solids, Institute of Chemistry, The Chinese Academy of Sciences, Beijing, 100080, P. R. China

Received: March 16, 2001; In Final Form: May 28, 2001

Photoinduced electron-transfer processes of C_{60} and C_{70} from alternating oligomers of phenylenevinylene derivatives (oligo(PV) derivatives) containing triphenylamine (TPA) or carbazole (Cz) and their monomer models (mono(PV) derivatives) in polar solvent have been investigated by nanosecond laser photolysis method with the observation of the transient absorption bands in the visible and near-IR regions. The transient species relating to the electron-transfer processes such as the triplet states of C_{60}/C_{70} ($^3C_{60}^*/^3C_{70}^*$), radical anions of C_{60}/C_{70} ($C_{60}^{\bullet-}/C_{70}^{\bullet-}$), and the radical cations of oligo(PV) derivatives and mono(PV) derivatives were detected in the region of 400−1600 nm. From their decays and rises, it is revealed that the electron-transfer process takes place via $^3C_{60}^*/^3C_{70}^*$ in polar solvent. The transient absorption bands of the radical cations of the PV derivatives revealed the delocalization of the radical-cation center (hole) along the PV backbone containing aromatic amines. In longer time scale, back electron transfer takes place from $C_{60}^{\bullet-}/C_{70}^{\bullet-}$ to the radical cations of mono(PV)/oligo(PV) derivatives; the back electron-transfer rate constants for oligo(PV) derivatives were smaller than those for mono(PV) derivatives. In the presence of octyl viologen dication (OV^{2+}), the electron of $C_{60}^{\bullet-}$ further transfers to OV^{2+}, yielding the viologen radical cation ($OV^{\bullet+}$), which prolongs the lifetimes of the cation radicals of mono(PV) and oligo(PV) derivatives. Although an accumulation of $OV^{\bullet+}$ was observed for the C_{60}/mono(PV)/OV^{2+} system, an almost completely reversible photosensitized electron-transfer/electron-mediating cycle was observed for C_{60}/oligo(PV)/OV^{2+}.

Introduction

Doping of C_{60} into the conductive polymer films such as poly-*N*-vinylcarbazole (poly(VCz)), polysilane, and poly-*p*-phenylenevinylene (poly(PV)) increases the photoinduced electric conductivity.[1−7] The mechanism and kinetics of electron-transfer processes of fullerenes have been investigated by photochemical techniques, such as laser flash photolysis, observing the transient absorption spectra in the visible/near-IR regions.[8−11] In the presence of electron-donor molecules, the radical anion of C_{60} ($C_{60}^{\bullet-}$) was usually produced via the triplet state of C_{60} ($^3C_{60}^*$) when the concentration of the donors are appropriately low, since the singlet excited state of C_{60} ($^1C_{60}^*$) changes to $^3C_{60}^*$ via intersystem crossing before the electron-transfer processes take place.[8−11] On the other hand, the photoinduced electron-transfer process via $^1C_{60}^*$ takes place in the concentrated donor solutions, polymer films, and poly(PV)-C_{60} linked molecule.[12−16]

In our previous papers, we showed that photoinduced electron transfer takes place from polymers with electron-donor abilities such as polysilane, polygermane, poly(VCz), and polythiophene to the triplet states of fullerenes in polar solvents.[17−19] However, the efficiencies of photoinduced electron transfer of these polymers via the triplet states of fullerenes are not always high.[17−19] In the present study, we tried to observe the photoinduced electron processes for PV modified with electron-donor groups such as aromatic amines as shown in Figure 1. The effects of the aromatic amines such as triphenylamine (TPA) and carbazole (Cz) incorporated in to the PV backbone on the efficiency of photoinduced electron-transfer processes were investigated. Comparison of the oligomers with the monomer models may be interesting to reveal the effect of repeating units of π-conjugation. The electron-mediating process from $C_{60}^{\bullet-}$ to octyl viologen dication (OV^{2+}) was also investigated to prove a photosensitized electron-transfer/electron-mediating cycle of C_{60}/PV/OV^{2+} systems. We can confirm the forward/backward electron-transfer processes and electron mediating processes by employing nanosecond laser flash photolysis with the visible/near-IR detectors.

Experimental Section

Materials. C_{60} and C_{70} were obtained from Term Co. in a purity of 99.9% and 99%, respectively. Mono(PV) derivatives and oligo(PV) derivatives were prepared by the methods described in the literature;[20−25] some characterization data for these compounds are reported in our previous papers.[20−22] The degrees of oligomerization of oligo(PV) derivatives (Table 1) are 3−7 except poly(MEH−PV) which contains ca. 860 monomer unit. Octyl viologen perchlorate (OV^{2+}, $2ClO_4^-$) was prepared from the commercially available chloride. Benzonitrile (BN) used as solvent was of HPLC grade. The solutions of C_{60}

* Author for correspondence. E-mail: ito@tagen.tohoku.ac.jp.
[†] Institute of Multidisciplinary Research for Advanced Materials, Tohoku University.
[‡] Laboratory of Organic Solids, Institute of Chemistry, The Chinese Academy of Sciences.

10.1021/jp011007l CCC: $20.00
Published on Web 07/18/2001

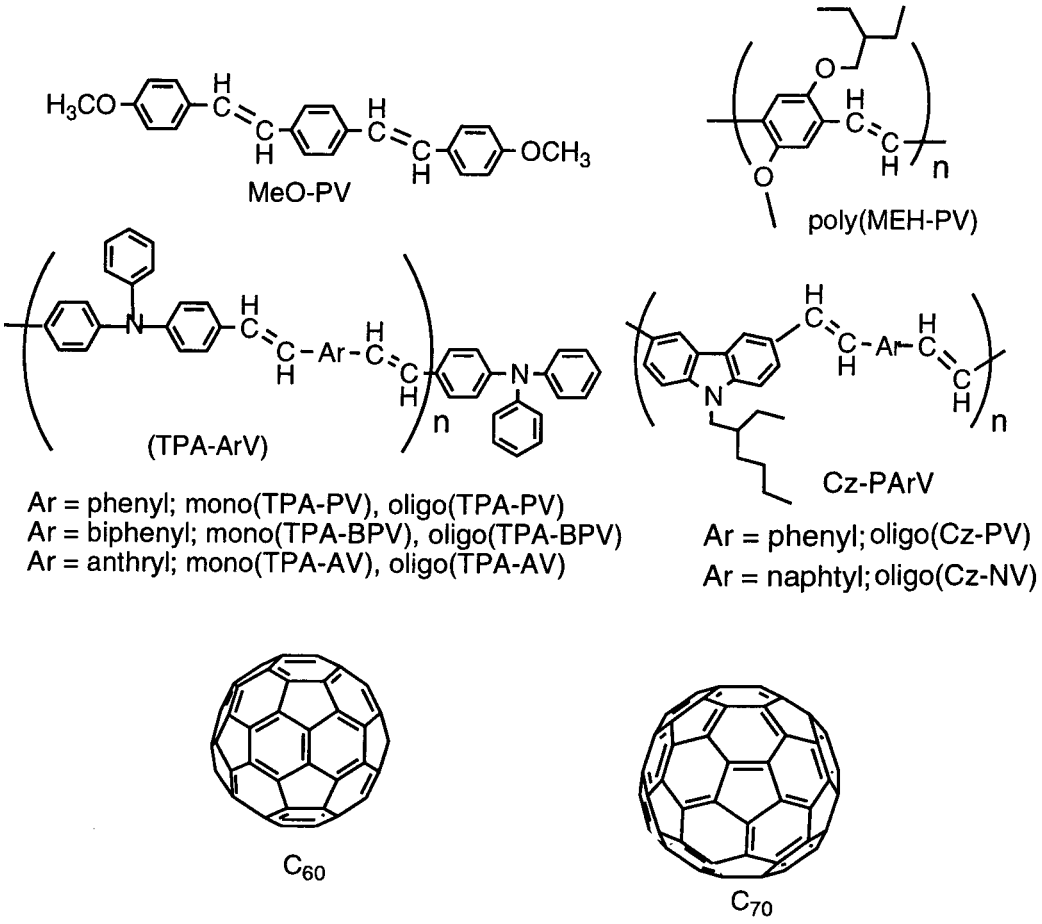

Figure 1. Molecular structures of donors and acceptors employed in the present study.

TABLE 1: Properties of Electron Donors (E_{ox}) and Degree of Oligomerization (n) and λ_{max} for Radical Cations in Transient Spectra Observed Photoexcitation of C_{60} in Deaerated BN

donors	E_{ox}/V[a]	n	λ_{max} of (donor)$^{\bullet+}$/nm ($\epsilon \times 10^{-3}$/M^{-1}cm^{-1})
MeO−PV	1.11	1	650 (43), 1380 (34)
poly(MEH−PV)	0.86	860	
TPA	1.00	1	700 (10)
mono(TPA−PV)	1.10	1	650 (29), 1600 (24)
oligo(TPA−PV)	1.10	3.8	600 (32), 1600 (30)
mono(TPA−BPV)	1.07	1	580 (29), 980 (17)
oligo(TPA−BPV)	1.01	6.6	550 (42), 1200 (24)
mono(TPA−AV)	1.07	1	580 (40), 1400 (12)
oligo(TPA−AV)	1.13	3.8	550 (89), 1400 (12)
EtCz	1.18	1	780 (10)
oligo(Cz−PV)	0.84	3.4	780 (19), 1500 (29)
oligo(Cz−NV)	0.86	4.1	730 (45), 1500 (30)

[a] Ag/AgCl reference electrode with 0.1 M of tetrabutylammonium perchlorate.

or C_{70} and oligo(PV) derivatives or mono(PV) derivatives were deaerated with Ar-bubbling before measurements.

Measurements. Transient absorption spectra in the visible/near-IR regions were observed by the laser-flash photolysis apparatus with an Nd:YAG laser (Quanta-Ray; 6 ns fwhm). C_{60} and C_{70} were excited with the SHG (532 nm) light. For time-scale measurements shorter than 10 μs, a Si−PIN photodiode module (400−600 nm) and a Ge-APD module (600−1600 nm) were employed as detectors for monitoring the light from a pulsed Xe-lamp.[26] For time-scale measurements longer than 10 μs, an InGaAs−PIN photodiode was used as a detector for monitoring light from a continuous Xe-lamp (150 W).[11] All experiments were carried out at 23 °C. Steady-state absorption spectra were measured with a JASCO/V-570 spectrophotometer.

Oxidation potentials (E_{ox}) of the PV derivatives were measured by cyclic voltammetry on a potentiostat (Hokuto Denko, HAB-151) in a conventional three-electrode cell equipped with Pt working and counter electrodes with Ag/AgCl reference electrode at scan rates of 100 mV/s. In each case, the solution contained 1.0 ∼ 5.0 mM of a sample with 0.1 M of tetrabutylammonium perchlorate (Nakarai Tesque). The solution was deaerated with Ar-bubbling before measurements. These E_{ox} values are summarized in Table 1, in addition to oligomerization numbers (n) defined in Figure 1.

Results and Discussion

Steady-State Absorption Spectra. In the steady-state UV/visible spectra, the mono(PV) and oligo(PV) derivatives show intense absorptions at wavelengths shorter than ca. 500 nm (Figure 2). The absorption spectrum of the mixture of C_{60} and mono(TPA-PV) is the same as the calculated spectrum of the corresponding components (Figure 2a), suggesting that the interaction between C_{60} and mono(TPA−PV) in the ground state is negligibly weak. For oligo(TPA−PV), similar spectra were observed as shown in Figure 2b. Also, no appreciable change was detected between the observed spectra of mixtures and calculated spectra for other systems. Although the PV derivatives show a weak absorption tail in the visible region (longer than 500 nm), the direct excitation of the PV derivatives with the 532 nm-laser light did not give any transient absorption bands in BN. On the other hand, the laser excitations of C_{60} and C_{70} with the 532 nm-laser light gave intense transient absorption bands due to their triplet states ($^3C_{60}$* and $^3C_{70}$*).[9−11,27] Thus,

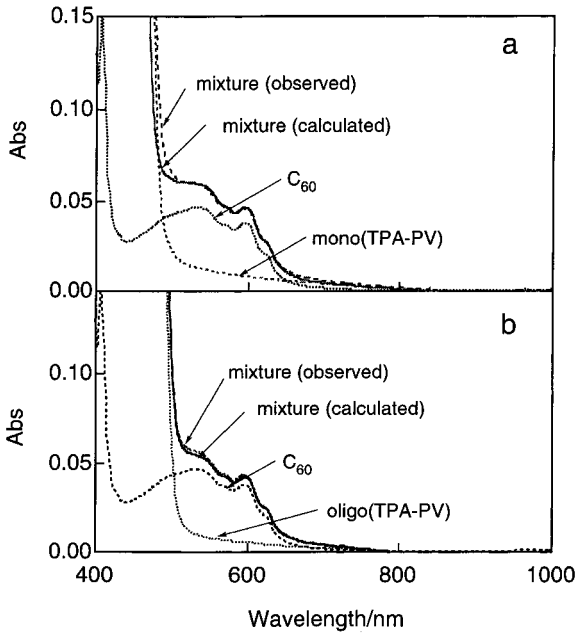

Figure 2. Steady-state absorption spectra of (a) C_{60} (0.1 mM), mono(TPA−PV) (1.0 mM), their mixture, and calculated one and (b) C_{60} (0.1 mM), oligo(TPA−PV) (1.0 mM), their mixture, and calculated one in BN (10 mm optical cell).

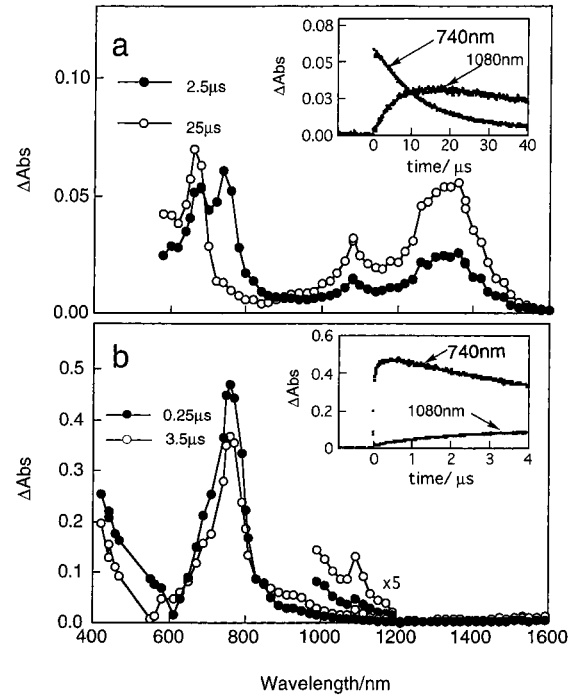

Figure 3. Transient absorption spectra obtained by laser photolysis of C_{60} (0.1 mM) in the presence of (a) MeO−PV (1.0 mM) and (b) poly(MEH−PV) (1.0 mM) in deaerated BN. Inset: Time profiles at absorption peaks.

the photophysical and photochemical processes of the excited states of C_{60} and C_{70} in the presence of mono(PV)/oligo(PV) derivatives may be observed using 532 nm-laser light as an exciting source.

Transient Absorption Spectra (C_{60}−PV Derivatives). Transient absorption spectra observed by the laser flash photolysis of C_{60} (0.1 mM) in the presence of MeO−PV (1.0 mM) in deaerated BN are shown in Figure 3a. A sharp absorption peak at 740 nm appearing immediately after the ns-laser pulse was attributed to $^3C_{60}$*.[9−11] With the decay of $^3C_{60}$*, the sharp absorption bands appeared at 660, 1080, and 1200−1400 nm. The absorption band at 1080 nm was characteristic of $C_{60}^{\bullet-}$.[9−11] The bands appearing at 660 nm showed the same rise time-profile as that in the 1200−1400 nm region, with the concomitant decay $^3C_{60}$*; thus, these absorption bands were assigned to the radical cation of MeO−PV (MeO−PV$^{\bullet+}$). The broad absorption bands in the near-IR region of MeO−PV$^{\bullet+}$ suggest that the radical-cation center (hole) delocalizes in the wide range of the molecule, since the absorption bands of the radical cations of styrene (614 nm) and *trans*-stilbene (760 nm) are reported to appear in the visible region.[28] Compared with the longest absorption of the radical cations of retinols (600 nm) and β-carotene (900 nm), the 1380 nm band of MeO−PV$^{\bullet+}$ is a longer wavelength.[29,30] This suggests that the phenyl groups between the vinyl groups in MeO−PV play a role to delocalize the radical-cation center of the PV moiety. The time profile of the transient absorption band of $^3C_{60}$* at 740 nm did not show the complete decay, because the decaying absorption of $^3C_{60}$* overlaps with the rising absorption of MeO−PV$^{\bullet+}$. The time profile of MeO−PV$^{\bullet+}$ shows that the absorbance reaches a maximum at ca. 10 μs under the experimental conditions described in Figure 3a. After reaching the maximum, the absorbance begins to decay, suggesting that back electron transfer takes place between the radical anion and radical cation.

In the case of poly(MEH−PV) (Figure 3b; 1.0 mM in monomer unit), the observed main transient band at 740 nm was attributed to $^3C_{60}$*, which decayed slowly accompanied by the slow rise of $C_{60}^{\bullet-}$. A weak absorption band showing rise was observed at 900−1000 nm, which may be attributed to poly(MEH−PV)$^{\bullet+}$. In comparison of Figure 3a with Figure 3b, it is shown that the yield of $C_{60}^{\bullet-}$ from poly(MEH−PV) is lower than that from MeO−PV, although the E_{ox} value of poly(MEH−PV) suggests its high electron-donor ability (Table 1). Thus, the low electron-donor ability of poly(MEH−PV) to $^3C_{60}$* may be related to the bulky alkyl groups on the phenyl rings of poly(MEH−PV).

Transient absorption spectra obtained by the laser flash photolysis of C_{60} in the presence of mono(TPA-PV) in BN are shown in Figure 4a. With the decay of $^3C_{60}$* at 740 nm, the rise of $C_{60}^{\bullet-}$ at 1080 nm was observed. The rise of mono(TPA-PV)$^{\bullet+}$ was observed at 620 nm and in the 1200−1600 nm region. In the case of TPA only, the weak absorption of TPA$^{\bullet+}$ was observed at 600 nm in addition to $C_{60}^{\bullet-}$ at 1080 nm, while no absorption was observed in the 1200−1600 nm region.[30] Thus, it is confirmed that the absorption band of 1200−1600 nm region is characteristic of the radical-cation center (hole) in the connected system of PV with TPA. Compared with MeO−PV$^{\bullet+}$, the near-IR band of mono(TPA−PV)$^{\bullet+}$ was broader and peak position shifted to longer wavelength, which may be resulted from the stronger electron-donor ability of the diphenylamine moiety than that of the methoxy group.

For oligo(TPA−PV) in BN, the transient absorption spectra and time profiles obtained by the laser photolysis of C_{60} are shown in Figure 4b. The spectral feature in the near-IR region is almost the same as that observed for mono(TPA−PV), which implies the similar electronic structure of mono(TPA−PV)$^{\bullet+}$ to oligo(TPA−PV)$^{\bullet+}$; the extent of the delocalization of both the radical cations (holes) is almost the same. A prominent difference between mono(TPA−PV) and oligo(TPA−PV) was observed for the time profiles. The decay rate of $^3C_{60}$* and the rise rates of $C_{60}^{\bullet-}$ and oligo(TPA−PV)$^{\bullet+}$ are quite faster than those of mono(TPA−PV)$^{\bullet+}$ when both donor concentrations are compared at their molecular-unit (i.e., each oligo(TPA−PV) contains 3.8 units of mono(TPA−PV)).

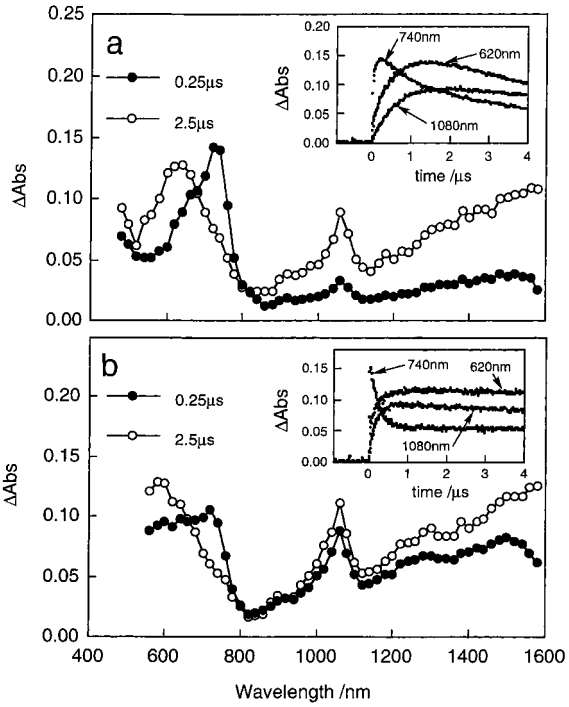

Figure 4. Transient absorption spectra obtained by laser photolysis of C_{60} (0.1 mM) in the presence of (a) mono(TPA−PV) (1.0 mM) and (b) oligo(TPA−PV) (1.0 mM) in deaerated BN. Inset: Time profiles at absorption peaks.

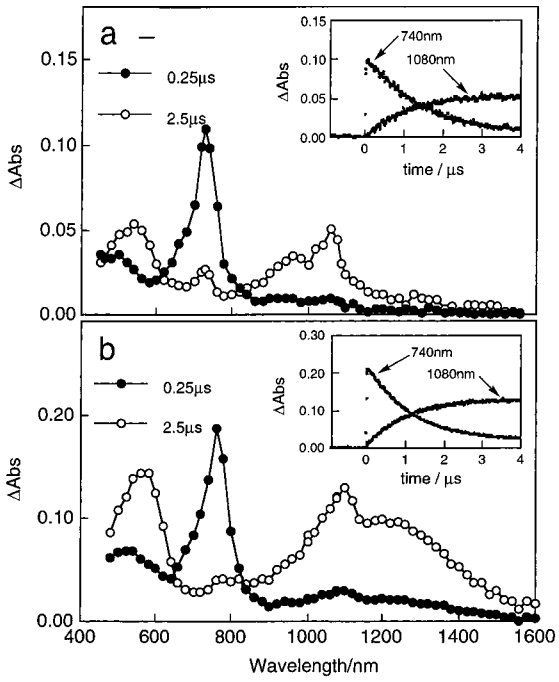

Figure 5. Transient absorption spectra obtained by laser photolysis of C_{60} (0.1 mM) in the presence of (a) mono(TPA−BPV) (1.0 mM) and (b) poly(TPA−BPV) (1.0 mM) in deaerated BN. Inset: Time profiles at absorption peaks.

When one of the phenyl rings of PV was replaced with the biphenyl group, the broad transient absorption band in the near-IR region disappeared as shown in Figure 5a (C_{60} and mono(TPA−BPV) system), although the rises of $C_{60}^{\bullet-}$ at 1080 nm and the radical-cation bands at 600 nm were observed with the concomitant decay of $^3C_{60}$* at 740 nm. The lack of the broad near-IR band of mono(TPA−BPV)$^{\bullet+}$ was attributed to the twisted structure of the biphenyl moiety, which cuts off the delocalization of the radical-cation center in the entire mono(TPA−BPV)$^{\bullet+}$. By the twisted structure, the near-IR bands around 1500−1600 nm seem to shift to shorter wavelengths down to 900 nm, which overlap with the 1080 nm band of $C_{60}^{\bullet-}$.

SCHEME 1

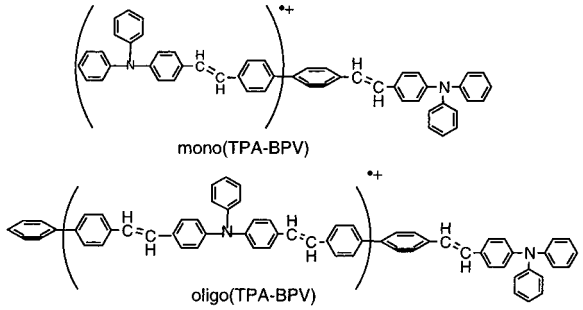

In the case of oligo(TPA−BPV) (Figure 5b), the new band appeared at 1250 nm overlapping with the 1080 nm band of $C_{60}^{\bullet-}$, with the concomitant decay of $^3C_{60}$* at 740 nm. This indicates that the 900 nm band of mono(TPA−BPV)$^{\bullet+}$ shifts to 1250 nm by oligomerization. This implies that the delocalization of the radical cation (hole) of oligo(TPA−BPV)$^{\bullet+}$ extends more widely than that of mono(TPA−BPV)$^{\bullet+}$, which is rationalized by the difference in the delocalization area as shown in Scheme 1.

In the transient absorption spectra observed by the laser excitation of C_{60} in the presence of mono(TPA−AV), the sharp transient absorption bands of mono(TPA−AV)$^{\bullet+}$ appeared at 580 nm with the decay of $^3C_{60}$*. Other transient bands of mono(TPA−AV)$^{\bullet+}$ in the near-IR region are broad, extending from 700 nm to the longer wavelength than 1600 nm. Compared with the transient absorption spectra of mono(TPA−PV), the intensity of the near-IR bands of mono(TPA−AV)$^{\bullet+}$ was weak, indicating that the conjugation of the radical cation (hole) is reduced by the replacement with the anthryl group in stead of the phenyl group, probably due to the steric hindrance between the anthracene moiety and the vinylene moieties. For C_{60}/oligo(TPA−AV), the transient spectrum of oligo(TPA−AV)$^{\bullet+}$ is quite broad and similar to that of mono(TPA−AV)$^{\bullet+}$, indicating that the delocalization of the hole (radical cation) is not improved by oligomerization, because the anthracene π-plane is not planer with the π-plane of the vinyl groups.

When the carbazole unit was introduced to the PV group instead of the TPA unit (oligo(Cz−PV)), the transient absorption spectral changes were quite similar to that of oligo(TPA−PV). The maximum of broad absorption of oligo(Cz−PV)$^{\bullet+}$ appeared at 1500 nm, which is slightly shorter than that of oligo(TPA−PV)$^{\bullet+}$ (1600 nm). On replacement of the phenyl group by the naphthyl group (oligo(Cz−NV)), the transient absorption in the near-IR region is similar to that of oligo(Cz−PV)$^{\bullet+}$. The naphthyl group does not reduce the delocalization of the cation-radical center. As was presumed from the E_{ox} values, electron-donor ability of oligo(Cz−PV) is higher than that of oligo-(TPA−PV), although the donor ability of ethylcarbazole (EtCz) is lower than that of TPA (Table 1).

Transient Absorption Spectra (C_{70}−PV Derivatives). Figure 6a shows the transient absorption spectra observed by the laser flash photolysis of C_{70} (0.1 mM) in the presence of mono(TPA−PV) (1.0 mM) in deaerated BN. The absorption band at 980 nm, which appeared immediately after the ns laser pulse, was attributed to $^3C_{70}$*.[31] With the decay of $^3C_{70}$*, the absorption bands appeared at 630 nm in addition to the broad bands in the 1000−1600 nm region, in which the 1380 nm band was ascribed to $C_{70}^{\bullet-}$.[31] Since the 630 nm band and broad band

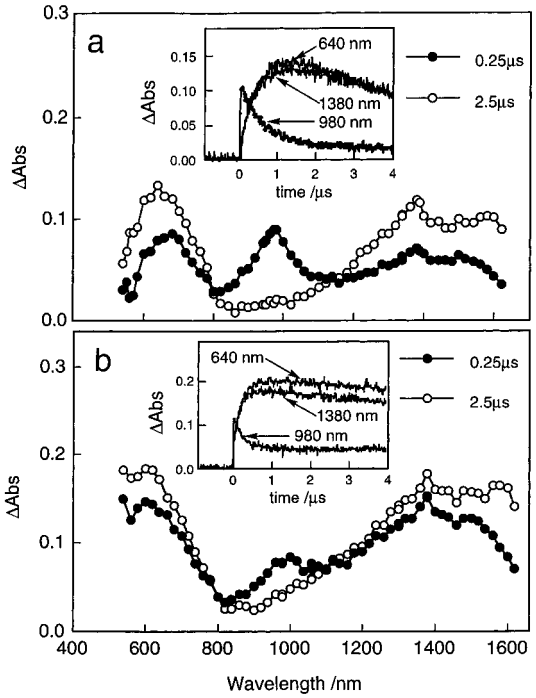

Figure 6. Transient absorption spectra obtained by laser photolysis of C_{70} (0.1 mM) in the presence of (a) mono(TPA−PV) (1.0 mM) and (b) oligo(TPA−PV) (1.0 mM) in deaerated BN. Inset: Time profiles at absorption peaks.

(1000−1600 nm) were the same as those observed for C_{60}/mono(TPA−PV) in Figure 4, they were assigned to mono-(TPA−PV)$^{\bullet+}$. In the presence of oligo(TPA−PV), the absorption band of $^3C_{70}$* at 980 nm decayed quickly, while other absorption bands in 500−1600 nm region of $C_{70}^{\bullet-}$ and oligo-(TPA−PV) $^{\bullet+}$ increased.

The spectral data of the cation radicals (λ_{max} and their molar extinction coefficients (ϵ_c)) are listed in Table 1. The ϵ_c values of the radical cations were evaluated on the basis of the reported molar extinction coefficient of $C_{60}^{\bullet-}$ (ϵ_A = 12 100 M^{-1} cm^{-1}) and $C_{70}^{\bullet-}$ (ϵ_A = 4000 M^{-1} cm^{-1}) as standards.[28−31] These ϵ_c values were necessary to calculate the back electron-transfer rate constants as described in the later section.

Kinetics and Quantum Yields for Electron Transfer. The initial part of each decay curve of $^3C_{60}$* at 740 nm was fitted with a single exponential, giving the first-order rate constant (k_{first}). The latter part of the decay curve deviated from the single exponential, because of the overlap with the rise components. The rise of $C_{60}^{\bullet-}$ was also curve-fitted with a single exponential, giving the k_{first} value. From the rises of the absorption bands of the radical cations, similar k_{first} values were also estimated.

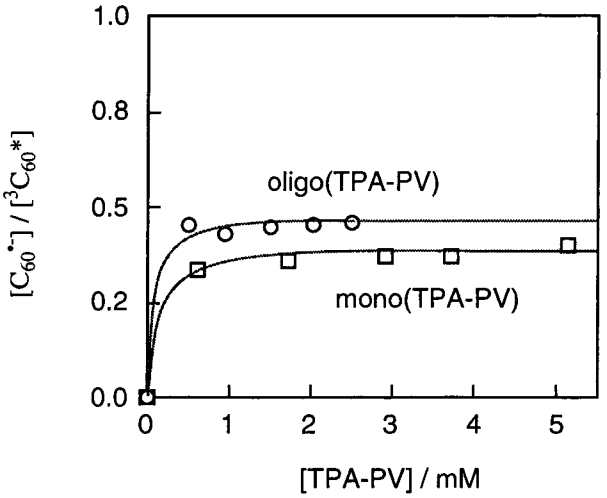

Figure 7. Plots of $[C_{60}^{\bullet-}]/[^3C_{60}*]$ vs concentrations of TPA−PV derivatives.

Compared with two methods, the analysis of the rise curve of $C_{60}^{\bullet-}$ gives more accurate values than that of the decay curve of $^3C_{60}$*, because the decay curves of $^3C_{60}$* overlap with the rise curves of the radical cations. In the plots of the k_{first} values with the donor concentrations, the slopes give the second-order rate constants (k_q), which are summarized in Table 2, in which the k_q value for poly(MEH−PV) was calculated on the basis of both monomer and polymer concentrations; it is difficult to compare directly these k_q values for poly(MEH−PV) with those of mono(PV) and oligo(PV) derivatives.

The quantum yield for the electron transfer (Φ_{et}) via $^3C_{60}$* can be evaluated from the plots of $[C_{60}^{\bullet-}]_{max}/[^3C_{60}*]_{max}$ vs the donor concentrations such as [mono(TPA−PV)] and [oligo-(TPA−PV)] as shown in Figure 7.[10,31] The saturated value corresponds to Φ_{et} (in Table 2). Since the quantum yields of the triplet excited state formation of C_{60} and C_{70} are almost unity,[9,10] these Φ_{et} values are almost same as the values evaluated from the photon number of the incident light.

From these findings, it is evident that $C_{60}^{\bullet-}$ and the cation radicals of PV derivatives are formed via $^3C_{60}$*, as shown in Scheme 2. The Φ_{et} values less than unity suggest that there are some routes for $^3C_{60}$* deactivation other than by the electron-

TABLE 2: Free-Energy Change (ΔG^o), Quenching Rate Constants (k_q), Quantum Yields (Φ_{et}), and Electron-Transfer Rate Constants (k_{et}) for Photoinduced Electron Transfer, and Back Electron-Transfer Rate Constants (k_{bet}) in Deaerated BN

acceptor	donors	$\Delta G°$ (kcal mol^{-1})	k_q ($M^{-1}s^{-1}$)	Φ_{et}	k_{et} ($M^{-1}s^{-1}$)	k_{bet} (M^{-1} s^{-1})
$^3C_{60}$*	MeO−PV	−4.73	7.6×10^8	0.40	3.0×10^7	8.4×10^9
$^3C_{60}$*	poly(MEH−PV)	−10.6	$(1.5 \times 10^8)^a$	0.04	$(6.3 \times 10^6)^a$	
$^3C_{60}$*	TPA	−7.36	1.6×10^9	0.60	9.6×10^8	1.3×10^{10}
$^3C_{60}$*	mono(TPA−PV)	−4.96	2.1×10^9	0.40	8.4×10^8	2.3×10^{10}
$^3C_{60}$*	oligo(TPA−PV)	−4.96	8.7×10^9	0.46	4.0×10^9	7.9×10^9
$^3C_{60}$*	mono(TPA−BPV)	−5.65	9.3×10^8	0.57	5.3×10^8	8.0×10^{10}
$^3C_{60}$*	oligo(TPA−BPV)	−7.05	1.2×10^{10}	0.46	5.5×10^9	1.1×10^{10}
$^3C_{60}$*	mono(TPA−AV)	−5.65	9.3×10^8	0.34	3.2×10^8	4.7×10^{10}
$^3C_{60}$*	oligo(TPA−AV)	−4.06	2.9×10^9	0.20	5.7×10^8	4.8×10^9
$^3C_{70}$*	mono(TPA−PV)	−4.96	3.2×10^9	0.58	1.2×10^9	1.5×10^{10}
$^3C_{70}$*	oligo(TPA−PV)	−4.96	7.5×10^9	0.85	6.4×10^9	6.8×10^9
$^3C_{60}$*	EtCz	−3.11	1.1×10^7	0.64	6.8×10^6	6.7×10^9
$^3C_{60}$*	oligo(Cz−PV)	−11.0	1.9×10^9	0.32	1.5×10^8	1.4×10^{10}
$^3C_{60}$*	oligo(Cz−NV)	−10.6	8.6×10^8	0.37	9.6×10^7	2.4×10^{10}

[a] These rate constants were calculated in monomer units; the rate constants for polymer units can be obtained by multiplying *n*.

SCHEME 2

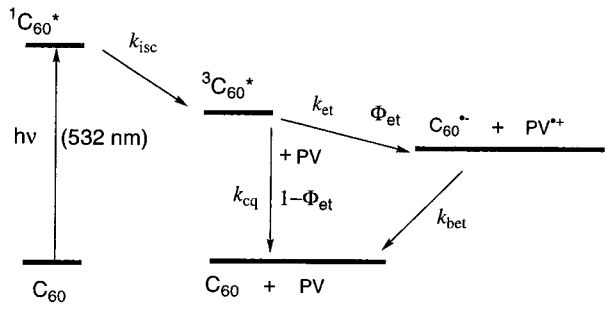

transfer process. For such deactivation processes, the collisional quenching process and excimer formation can be considered, which is denoted as k_{cq} in Scheme 2.[10,32]

Within the C_{60} donor systems, EtCz and TPA have high Φ_{et} values, which are decreased by the connection with the PV moiety. This indicates that the PV-moiety facilitates the $^3C_{60}$* deactivation via collisional encounter complex and/or exciplex. For C_{60} and C_{70}, the Φ_{et} value of mono(TPA−PV) is lower than that of oligo(TPA−PV). On the other hand, the opposite tendency was observed for TPA−AV and TPA−BPV. The Φ_{et} values for the C_{70} systems are higher than those for the C_{60} systems.

The rate constants of electron transfer (k_{et}) can be evaluated from the relation, $k_{et} = \Phi_{et}\, k_q$, which are summarized in Table 2. It is found that the k_{et} value for TPA is quite larger than that for MeO−PV, which is in agreement with the tendency of the E_{ox} values. The E_{ox} values and free-energy changes for electron transfer ($\Delta G°$) in Tables 1 and 2 predict lower electron-donor abilities of mono(TPA−PV) and oligo(TPA−PV) than that of TPA;[32] however, the observed k_{et} value for mono(TPA−PV) is as large as that of TPA. Furthermore, the observed k_{et} value for oligo(TPA−PV) is larger than that of TPA. This may be attributed to the larger electron-transfer cross section of oligo(TPA−PV) with $^3C_{70}$* compared with those of TPA and mono(TPA−PV). Since the initial concentration of $^3C_{60}$* is as low as 10^{-5} M, the possibility that many $^3C_{60}$* units attack on each oligo(TPA−PV) is low, except poly(MEH−PV).

In the case of oligo(Cz−PV) and oligo(Cz−NV), a considerable increase in k_{et} values would be anticipated from negatively large $\Delta G°$ values. Indeed, the observed k_{et} values for oligo(Cz−PV) and oligo(Cz−NV) are far greater than that of EtCz. This indicates that π-conjugation of the PV and NV moieties with the Cz moiety in oligo(Cz−PV) and oligo(Cz−NV) increases the k_{et} values as predict. Compared with MeO−PV, the Cz moiety increases considerably the electron-donor ability of the PV moiety.

For mono(TPA−PV) and oligo(TPA−PV), we can compare the reactivities between $^3C_{60}$* and $^3C_{70}$*; the k_{et} values of $^3C_{70}$* are higher than those of $^3C_{60}$* (Table 2), which is important in view of application to some devices, since it is not necessary to separated C_{70} exclusively from the mixture of C_{60} and C_{70}.

Back Electron Transfer. In BN, the intensities of $C_{60}^{\bullet-}$ at 1080 nm begin decaying slowly after reaching maximal concentration as shown in Figures 3a, 4a, and 7a,b. Since Figure 8 was depicted in the long time scale, only the decay of $C_{60}^{\bullet-}$ was observed. These decays obey second-order kinetics as shown in inset of Figure 8. The absorption intensity of mono(TPA−PV)$^{\bullet+}$ or oligo(TPA−PV)$^{\bullet+}$ also began to decay in the same rates with that of $C_{60}^{\bullet-}$. These decays in polar solvents can be attributed to the back electron-transfer process between the freely solvated anion radical and cation radical (Scheme 2).

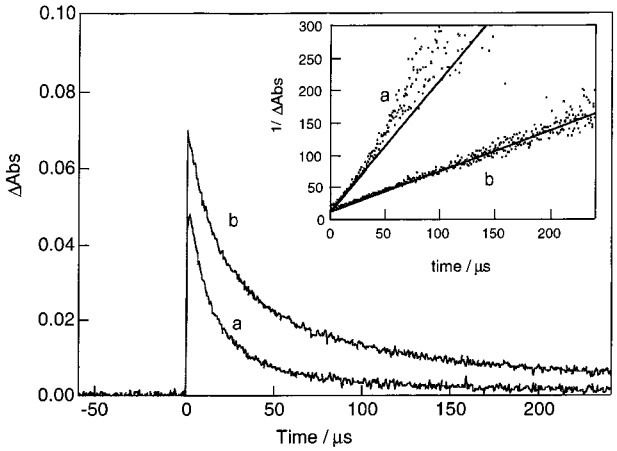

Figure 8. Decay time profiles of $C_{60}^{\bullet-}$ and second-order plots (inset) in the presence of (a) mono(TPA−PV)$^{\bullet+}$ and (b) oligo(TPA−PV)$^{\bullet+}$ in deaerated BN.

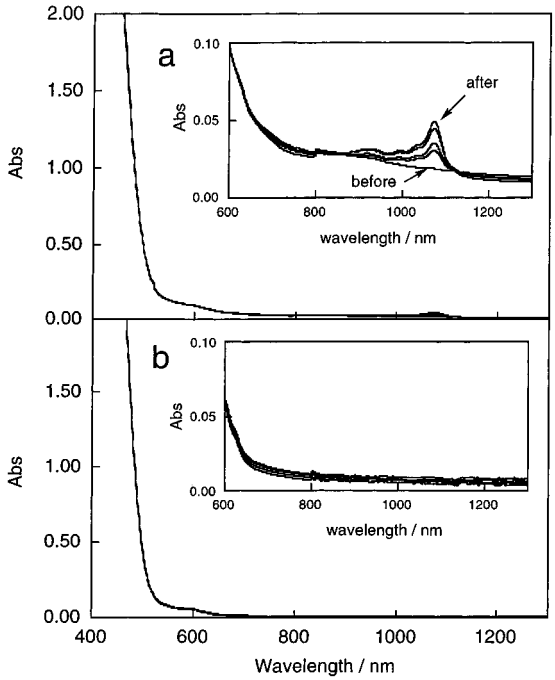

Figure 9. Steady-state absorption spectra before and after photoirradiation of C_{60} (0.1 mM) in the presence of (a) mono(TPA−AV) (1.0 mM) and (b) oligo(TPA−AV) (1.0 mM) in deaerated BN (10 mm optical cell).

From the slopes of the second-order plots (inserted plots in Figure 8), the ratio of the rate constant to the molar extinction coefficient (k_{bet}/ϵ_A) can be obtained. When the absorptions of $C_{60}^{\bullet-}$ and radical cation overlapped, the molar extinction coefficients ($\epsilon_A + \epsilon_C$) were employed. On substituting the reported ϵ_A and estimated ϵ_C in Table 1, the k_{bet} values in BN were evaluated as listed in Table 2. The k_{bet} value for mono(TPA−PV)$^{\bullet+}$ (2.3×10^{10} M^{-1} s^{-1}) is far larger than the k_{bet} value for oligo(TPA−PV)$^{\bullet+}$ (7.9×10^{9} M^{-1} s^{-1}). For other monomer−oligomer pairs, similar tendency was observed (last column in Table 2). This may be reasonable, because the radical-cation center (hole) in oligomer delocalizes in the whole oligomer chain apart from $C_{60}^{\bullet-}$, which retards the encounter of $C_{60}^{\bullet-}$ with the hole again. This finding is important in relation to the photoinduced electric conductivity in the C_{60}/C_{70}-doped oligo(TPA−PV) derivatives.

Reactions after Electron Transfer. After repeated irradiation of C_{60} (or C_{70}) with the laser light at 532 nm in the presence of

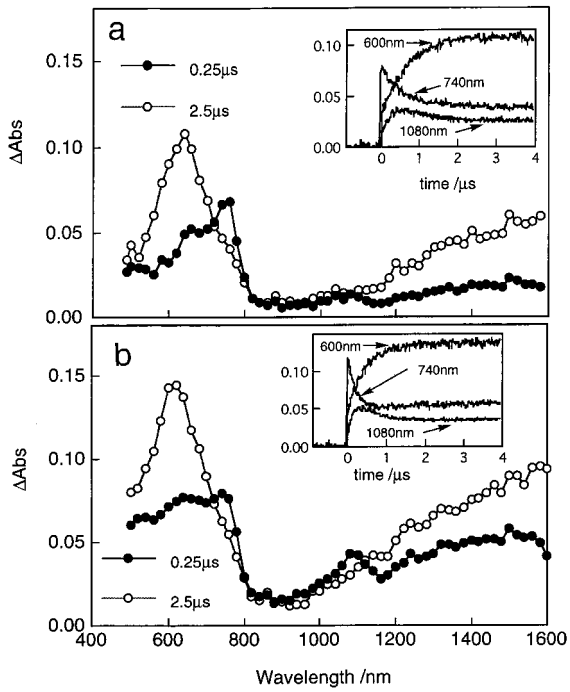

Figure 10. Transient absorption spectra obtained by laser photolysis of C_{60} (0.1 mM) in the presence of (a) mono(TPA−PV) (1.0 mM) and OV^{2+} (0.5 mM) and (b) oligo(TPA−PV) (1.0 mM) and OV^{2+} (0.5 mM) in deaerated BN. Inset: Time profiles at representative absorption peaks.

SCHEME 3

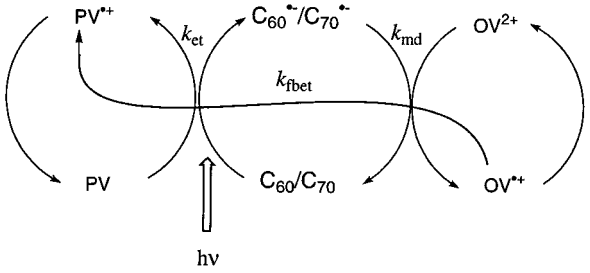

mono(TPA−PV) and oligo(TPA−PV) in deaerated BN, the steady-state absorption spectra did not change much (Figure 9). This indicates that the systems of C_{60}/C_{70} and PV derivatives are considerably stable for the photoirradiation. In the case of the C_{60}/mono(TPA−PV) system, small changes became appreciable after magnification of the absorbance (inset of Figure 9a). A small amount of $C_{60}^{\bullet-}$ seems to be persistent in the system of C_{60} and mono(TPA−PV)$^{\bullet+}$ after the light is cut off. This implies that mono(TPA−PV)$^{\bullet+}$ reacts into less electron deficient substances; the intramolecular and intermolecular cyclization reactions of mono(TPA−PV)$^{\bullet+}$ are candidates for such reactions. On the other hand, such persistent $C_{60}^{\bullet-}$ was not observed for the C_{60}/oligo(TPA−PV) system, suggesting that the degradation of oligo(TPA−PV)$^{\bullet+}$ is more difficult than that of mono(TPA−PV)$^{\bullet+}$. The same tendency was observed for mono(TPA−AV) and oligo(TPA−AV).

Electron Mediating Process to Viologen Dication. In the presence of mono(TPA−PV) and octyl viologen dication (OV^{2+}), laser flash irradiation of C_{60} induces, at first, electron transfer from mono(TPA−PV) to $^3C_{60}$*, which was confirmed by the rapid decay of $^3C_{60}$* and by the rapid rise of $C_{60}^{\bullet-}$, as shown in Figure 10a. The produced $C_{60}^{\bullet-}$ successively donates its excess electron to OV^{2+}, which was also indicated by the decay of $C_{60}^{\bullet-}$ at 1080 nm and the rise of $OV^{\bullet+}$ at 600 nm. Successive formation of $OV^{\bullet+}$ was indicated by the relatively slow rise compared with that of $C_{60}^{\bullet-}$. During these processes, mono(TPA−PV)$^{\bullet+}$ increased rapidly and remained almost constant during ca. 10 μs. In this case, C_{60} acts as an electron mediator in addition to a photosensitizing electron acceptor as illustrated in Scheme 3.[33] In the case of oligo(TPA−PV), the slow rise of $OV^{\bullet+}$ was also observed with the loss of $C_{60}^{\bullet-}$ at ca. 2.5 μs (Figure 10b).

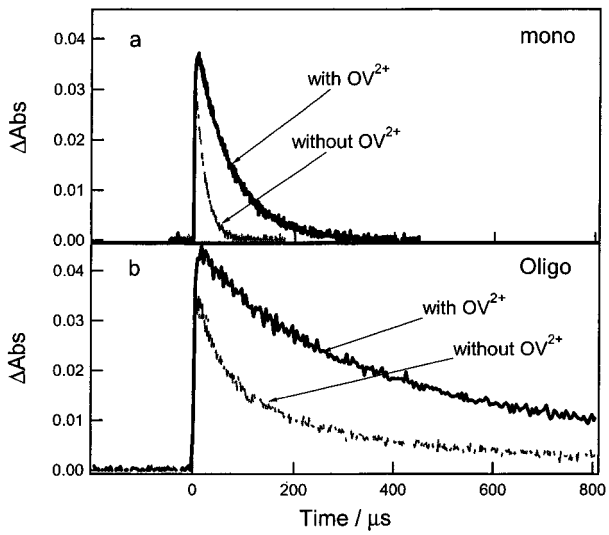

Figure 11. Time profiles at 1600 nm obtained by laser flash photolysis of C_{60} (0.1 mM) in the presence of (a) mono(TPA−PV) (1.0 mM) with OV^{2+} (0.5 mM) and without OV^{2+} and (b) oligo(TPA−PV) (1.0 mM) with OV^{2+} (0.5 mM) and without OV^{2+} in deaerated BN (10 mm optical cell).

The rate constants for electron mediating processes (k_{md}) from $C_{60}^{\bullet-}$ to OV^{2+} were evaluated from the dependence of the decay rates of $C_{60}^{\bullet-}$ on the concentration of OV^{2+} to be 6.6×10^8 M^{-1} s^{-1} for mono(TPA−PV) and 3.4×10^9 M^{-1} s^{-1} for oligo(TPA−PV). The observed trend suggests that some interactions exist between $C_{60}^{\bullet-}$ and mono(TPA−PV)$^{\bullet+}$, which retards the electron release to OV^{2+}. This interaction of mono(TPA−PV)$^{\bullet+}$ with $C_{60}^{\bullet-}$ may be the same with that presumed from the k_{bet} values.

Figure 11 shows the long-time decay of mono(TPA−PV)$^{\bullet+}$/oligo(TPA−PV)$^{\bullet+}$ at 1600 nm in the presence and absence of OV^{2+}. In the absence OV^{2+}, the decays are attributed to back electron transfer from $C_{60}^{\bullet-}$ to mono(TPA−PV)$^{\bullet+}$/oligo(TPA−PV)$^{\bullet+}$, which gave the same k_{bet} values as evaluated from Figure 8, while in the presence of OV^{2+}, the decays are attributed to final back electron transfer (k_{fbet}) from $OV^{\bullet+}$ to mono(TPA−PV)$^{\bullet+}$/oligo(TPA−PV)$^{\bullet+}$, as shown in Scheme 3. For both mono(TPA−PV)$^{\bullet+}$ and oligo(TPA−PV)$^{\bullet+}$ systems, the decays of the radical cations in the presence of OV^{2+} are slowed compared with those in the absence of OV^{2+}. This means that the lifetimes of the charge separate states between mono(TPA−PV)$^{\bullet+}$/oligo(TPA−PV)$^{\bullet+}$ and OV^+ are quite longer than those between mono(TPA−PV)$^{\bullet+}$/oligo(TPA−PV)$^{\bullet+}$ and $C_{60}^{\bullet-}/C_{70}^{\bullet-}$. This may be caused by repulsion between positively charged mono(TPA−PV)$^{\bullet+}$/oligo(TPA−PV)$^{\bullet+}$ and $OV^{\bullet+}$. The k_{fbet} values were evaluated from the slopes of the second-order plots and the molar extinction coefficients in Table 1. The k_{fbet} values for mono(TPA−PV)$^{\bullet+}$ and oligo(TPA−PV)$^{\bullet+}$ were evaluated to be 5.4×10^9 and 1.7×10^9 M^{-1} s^{-1}, respectively. Similar k_{fbet} values were evaluated from the decay of $OV^{\bullet+}$ at 600 nm in the long time-scale measurements using the reported molar extinction coefficient of $OV^{\bullet+}$ at 600 nm.[34] It is confirmed that these k_{fbet} values are smaller than the k_{bet} values in each system. These k_{fbet} values for oligo(TPA−PV)$^{\bullet+}$ are smaller than those

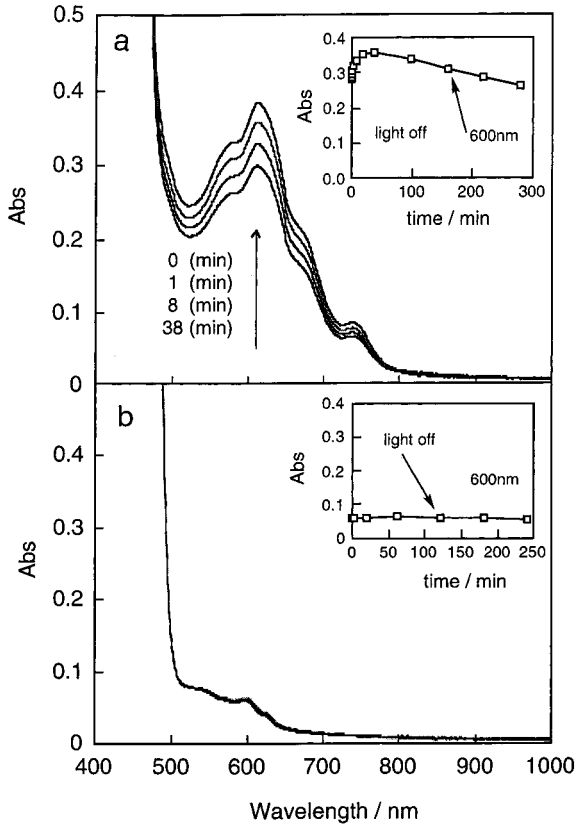

Figure 12. Steady-state absorption spectra observed by photoirradiation of C_{60} (0.1 mM) in the presence of (a) mono(TPA−PV) (1.0 mM) and OV^{2+} (0.5 mM) and (b) oligo(TPA−PV) (1.0 mM) and OV^{2+} (0.5 mM) in deaerated BN (10 mm optical cell).

for mono(TPA−PV)$^{\bullet+}$. This tendency is the same as k_{bet} values. The wide delocalization of the cation-radical center along oligo(TPA−PV) may retard the back electron transfer to $OV^{\bullet+}$ compared with narrow radical-cation delocalized within mono-(TPA−PV).

When $OV^{\bullet+}$ works with electrodes and catalysts efficiently, it is necessary to have a lifetime long enough to transfer its excess electron. Therefore, it is considered that the oligo(TPA−PV) system is superior to the mono(TPA−PV) system in many kinetic aspects, such as larger k_{et} and k_{md} and smaller k_{bet} and k_{fbet}.

To investigate the stability of the photosensitized electron-transfer/electron-mediating systems, the steady-state measurements were performed for the C_{60}/mono(TPA−PV)/OV^{2+} and C_{60}/oligo(TPA−PV)/OV^{2+} systems as shown in Figure 12. In the case of the C_{60}/mono(TPA−PV)/OV^{2+} system, $OV^{\bullet+}$ was produced persistently during the steady-state photolysis, while the C_{60}/oligo(TPA−PV)/OV^{2+} system did not produce persistent $OV^{\bullet+}$ at all. The formation of the persistent $OV^{\bullet+}$ can be ascribed to the persistent formation of $C_{60}^{\bullet-}$ in the C_{60}/mono(TPA−PV) system as shown in Figure 9, while the absence of persistent $OV^{\bullet+}$ in the C_{60}/oligo(TPA−PV)/OV^{2+} system is related to the absence of persistent $C_{60}^{\bullet-}$ in the C_{60}/oligo(TPA−PV) system. These findings indicate that the formation of the persistent $OV^{\bullet+}$ is ascribed to some equilibrium reasons, but not to kinetic reasons. For the recycling of the components in photosensitized electron-transfer/electron-mediating cycle, the C_{60}/oligo(TPA−PV)/OV^{2+} system is better than the C_{60}/mono(TPA−PV)/OV^{2+} system, since mono(TPA−PV) would be consumed during steady-state photolysis. Although the persistent $OV^{\bullet+}$ was not observed for the C_{60}/oligo(TPA−PV)/OV^{2+} system during steady-state photolysis, the transient measurements in this study clearly proved that photosensitized electron-transfer/electron-mediating cycle is working in the C_{60}/oligo(TPA−PV)/OV^{2+} system with longer charge-separated lifetime.

Conclusion

It is shown in the present study that TPA−PV and Cz−PV are good electron donors to $^3C_{60}$* and $^3C_{70}$* in BN. The transient spectra in the near-IR region indicate that the radical cation centers (holes) of the PV derivatives delocalize in the wide region of the PV molecules. For these cases, C_{60} and C_{70} act as electron mediators after photosensitized electron transfer in the presence of viologen. Although the C_{60}/oligo(PV) and C_{60}/oligo(PV)/OV^{2+} systems were photostable, slight degradation was observed during the photoillumination to the C_{60}/mono(PV) and C_{60}/mono(PV)/OV^{2+} systems. Since the photosensitized electron-acceptor ability of C_{70} is similar to that of C_{60}, the crude C_{60} powder including C_{70} can be used as dopant for the photoelectric-conductive devises without complete exclusion.

Acknowledgment. The present work was partly supported by a Grant-in-Aid on Priority-Area-Research on Laser Chemistry of Single Nanometer Organic Particle (No. 10207202) and a Grant-in-Aid (No. 11440211) from the Ministry of Education, Science, Culture and Sports.

References and Notes

(1) Wang, Y. *Nature* **1992**, *356*, 585.
(2) Wang, Y.; West, R.; Yuan, C.-H. *J. Am. Chem. Soc*. **1993**, *115*, 3844.
(3) Yoshino, K.; Xiao, H.-Y.; Muro, K.; Kiyomatsu, S.; Morita, S.; Zakhidov, A. A.; Noguchi, T.; Ohinishi, T. *Jpn. J. Appl. Phys*. **1993**, *32*, L357.
(4) Yoshino, K.; Xiao, H.-Y.; Morita, S.; Kawai, T.; Zakhidov, A. A. *Solid State Commun.* **1993**, *85*, 85.
(5) Sariciftci, N. S.; Baum, D.; Zhang, C.; Srdanov, V. I.; Heeger, A. J.; Stucky, G.; Wudl, F. *Appl. Phys. Lett*. **1963**, *62*, 585.
(6) Smilowitz, L.; Sariciftci, N. S.; Wu, R.; Gettinger, C.; Heeger, A. J.; Wudl, F. *Phys. Rev. B*. **1994**, *47*, 13835.
(7) Halls, J. J. N.; Pichler, K.; Friend, R. H.; Moratti, S. C.; Holmes, A. B. *Appl. Phys. Lett*. **1996**, *68*, 3120.
(8) Ebbesen, T. W.; Tanigaki, K.; Kuroshima, S. *Chem. Phys. Lett*. **1991**, *181*, 501.
(9) Nonell, S.; Arbogast, J. W.; Foote, C. S. *J. Phys. Chem*. **1992**, *96*, 4169.
(10) Steren, C. A.; von Willigen, H.; Biczok, L.; Gupta, N.; Linschitz, H. *J. Phys. Chem*. **1996**, *100*, 8920.
(11) Fujitsuka, M.; Yahata, Y.; Watanabe, A.; Ito, O. *Polymer* **2000**, *41*, 2807.
(12) Sension, R.; Szarka, A. Z.; Smith, G. R.; Hochstrasser, R. M. *Chem. Phys. Lett*. **1991**, *185*, 179.
(13) Ghosh, H. N.; Pal, H.; Sapre, A. V.; Mittal, J. P. *J. Am. Chem. Soc*. **1993**, *115*, 11722.
(14) Sauvè, G.; Dimitrijevic, N. M.; Kamat, P. V. *J. Phys. Chem*. **1995**, *99*, 1199.
(15) Itaya, A.; Suzuki, I.; Tsuboi, Y.; Miyasaka, H. *J. Phys. Chem. B* **1997**, *101*, 5118.
(16) Stalmach, U.; de Bore, B.; Videlot, C.; van Hutten, P. F.; Hadziioannou, G. *J. Am. Chem. Soc.* **2000**, *122*, 5464.
(17) Watanabe, A.; Ito, O. *J. Phys. Chem*. **1994**, *98*, 7736.
(18) Watanabe, A.; Ito, O.; Mochida, K. *Organometallics* **1995**, *14*, 4281.
(19) Matsumoto, K.; Fujitsuka, M.; Sato, T.; Onodera, S.; Ito, O. *J. Phys. Chem. B* **2000**, *104*, 11632.
(20) Zheng, M.; Bai, F.; Zhu, D. *Polym. Adv. Technol*. **1999**, *10*, 476.
(21) Zheng, M.; Bai, F.; Zhu, D. *J. Appl. Polym. Sci*. **1999**, *74*, 3351.
(22) Bai, F.; Zheng, M.; Zhu, D. *Thin Solid Films* **2000**, *363*, 118.
(23) Xue, M.; Huang, D.; Liu, Y. *Synth. Met*. **2000**, *110*, 203.
(24) Pfeiffer, S.; Rost, H.; Horhold, H. *Macromol. Chem. Phys*. **1999**, *200*, 2471.
(25) Eckert, J.; Armaroli, N.; Barigelletti, F.; Ceroni, P.; Nicoud, J.; Nierengarten, J. *Fullerenes 2000, Electrochemistry and Photochemistry;* Fukuzumi, S., D'Souza, F., Guldi, D. M., Eds.; The Electrochemical Society: Pennington, NJ, 2000; Vol. 8, pp 256−266.
(26) The Ge−APD detector employed in this study showed slow time response when the absorbance change is large (i.e., time-profile at 740 nm

in inset of Figure 3b), although the time response is quite good at appropriate absorbance. The kinertic analysis and quantum yield determination were performed under these appropriate conditions.

(27) Sasaki, Y.; Konishi, T.; Fujitsuka, M.; Ito, O. *Phys. Chem. Chem. Phys*. **1999**, *1*, 4555.

(28) Shida, T. Electronic Absorption Spectra of Radical Ions. In *Physical Science Data* 34, Elsevier: Amsterdam, 1988,

(29) Sasaki, Y.; Fujitsuka, M.; Watanabe, A.; Ito, O. *J. Chem. Soc., Faraday Trans*. **1997**, *9*, 4275

(30) Yahata, Y.; Ysasaki, Y.; Fujitsuka, M.; Ito, O. *J. Photosci*. **1999**, *6*, 117.

(31) Alam, M. M.; Watanabe, A.; Ito, O. *Bull. Chem. Soc. Jpn*. **1997**, *70*, 1833.

(32) Heath, G. A.; McGray, J. R. E.; Martin, R. L. *J. Chem. Soc., Chem. Commun*. **1992**, 1272.

(33) Rehm, D.; Weller, A. *Isr. J. Chem*. **1970**, *8*, 259.

(34) Konishi, T.; Toba, Y.; Usui, Y.; Ito, O. *J. Phys. Chem. A* **1999**, *103*, 9938.